HHS Public Access

Author manuscript

Nat Cell Biol. Author manuscript; available in PMC 2011 October 01.

Published in final edited form as:

Nat Cell Biol. 2011 April ; 13(4): 461–468. doi:10.1038/ncb2202.

The cilia protein IFT88 is required for spindle orientation in mitosis

Benedicte Delaval[1], **Alison Bright**[1], **Nathan Lawson**[2], and **Stephen Doxsey**[1,3]

[1] Program in Molecular Medicine, University of Massachusetts Medical School, Worcester Massachusetts 01605

[2] Program in Gene Function and Expression, University of Massachusetts Medical School, Worcester Massachusetts 01605

Abstract

Cilia dysfunction has long been associated with cyst formation and ciliopathies[1]. More recently, misoriented cell division has been observed in cystic kidneys[2], but the molecular mechanism leading to this abnormality remains unclear. Proteins of the intraflagellar transport (IFT) machinery are linked to cystogenesis and required for cilia formation in non-cycling cells[3], [4]. Several IFT proteins also localize to spindle poles in mitosis[5]–[8] suggesting uncharacterized functions for these proteins in dividing cells. Here, we show that IFT88 depletion induces mitotic defects in human cultured cells, in kidney cells from the IFT88 mouse mutant *Tg737*^{orpk} and in zebrafish embryos. In mitosis, IFT88 is part of a dynein1-driven complex that transports peripheral microtubule (MT) clusters containing MT-nucleating proteins to spindle poles to ensure proper formation of astral MT arrays and thus, proper spindle orientation. This work identifies a mitotic molecular mechanism for a cilia protein in the orientation of cell division and thus, has important implications for the etiology of ciliopathies.

In non-cycling cells, centrosomes (basal bodies) contribute to the assembly of primary cilia[9] through intraflagellar transport, an intracellular motility system in which protein complexes are transported bidirectionally along the cilium[10]–[12]. During mitosis, centrosomes (spindle poles) participate in the organization and orientation of the spindle[13]–[15]. In this context, astral MTs interact with spindle MTs to facilitate chromosome segregation[13] and with the cell cortex to orient the spindle[14], [15]. One of the best-studied IFT proteins, IFT88, which was first characterized for its role in cilia formation and polycystic kidney disease[3], [16]–[19], also localizes to spindle poles during mitosis[6].

[3]Correspondence should be addressed to S.D. Stephen.Doxsey@umassmed.edu, University of Massachusetts Medical School, Program in Molecular Medicine, 373 Plantation Street, Suite 210, Worcester, MA 01605, Phone: 508-856-1613; Fax: 508-856-4289.

Supplementary Informations

Supplemental Data includes 7 figures and 5 movies.

Author Contributions

B.D. and S.D. wrote the manuscript. B.D. conceived and planned the experimental work. B.D. and A.B. carried out the experimental work and analyzed the data. N.L provided the zebrafish facility and helped plan and guide the zebrafish experimental work.

To test for mitotic functions of IFT88, the protein was depleted in several experimental systems. In HeLa cells, defects in mitosis were first suggested by an increased mitotic index and delayed mitotic progression (Supplementary Information Fig. S1a–e). Closer inspection revealed spindle pole disruption, chromosome misalignment and spindle misorientation (Fig. 1a, b). The spindle angle relative to the cell-substrate adhesion plane (Fig. 1c, d)[15] of most IFT88-depleted cells (~80%) was greater than 10° whereas control spindles were usually parallel to the substratum (Fig. 1d), demonstrating a critical role for IFT88 in spindle orientation. Time-lapse imaging showed that spindle misorientation resulted in misoriented cell divisions, where one daughter cell divided outside the plane of the substratum, thus delaying adherence to the substrate (Fig. 1e, f). Despite misorientation, spindles were largely bipolar (Fig. 1a) and cells ultimately progressed through division (Fig. 1f; Supplementary Information Fig. S1d). Based on the role of IFT88 in cystic kidney formation[3], IFT88 disruption was examined in kidney cell lines by siRNA (porcine LLC-PK1, Supplementary Information, Fig. S2a–c) and by mutation (murine *Tg737*^{orpk}, Fig. 1g; Supplementary Information, Fig. S2d) and showed similar mitotic defects. In zebrafish embryos, IFT88 depletion by morpholino oligonucleotides known to induce ciliopathies[18] also resulted in mitotic defects including misoriented spindles (Fig. 1h; Supplementary Information, Fig. S2e). These results demonstrate a conserved mitotic role for IFT88 in spindle and cell division orientation.

We next examined the structural underpinnings of spindle misorientation induced by IFT88 depletion. The most notable defect was a significant loss and shortening of astral MTs, which did not contact the cell cortex, a requirement for force generation during spindle orientation (Fig. 2a, b). This phenotype was consistently observed in different experimental systems (Fig. 2a, b; Fig. 1g), demonstrating a conserved role for IFT88 in the formation of astral MT arrays.

In centrosome containing cells, astral MT arrays arise from both centrosome-based nucleation and transport of MT clusters to the poles from the periphery[20], [21]. To define the role of IFT88 in the assembly of astral MT arrays, we tested the contribution of the protein in both processes. A role for IFT88 in MT nucleation was first suggested by loss of MT nucleating components, γtubulin and EB1[13], [22]–[25], from spindle poles following IFT88 depletion (Fig. 2c, d; Supplementary information Fig. S3a, b); EB1 depletion did not affect IFT88 pole localization (Supplementary information Fig. S3c). The similarities in mitotic phenotypes induced by depletion of IFT88, EB1 or γtubulin (spindle pole defects, reduced astral MTs and misoriented spindle; Fig. 1)[15], [23]–[25], and the mitotic interaction of IFT88 with EB1 and γtubulin (Fig. 2e), supported the idea that these proteins may co-function in mitosis. More specifically, the impaired recruitment of γtubulin to spindle poles in IFT88 depleted cells following MT regrowth (Fig. 2f) suggested a role for IFT88 in the recruitment of MT nucleating components to spindle poles. Consistent with the polar loss of MT nucleating proteins, IFT88 depletion decreased MT nucleation, but the effect was modest when compared to the dramatic disruption of astral MTs (Fig. 2g, h; Supplementary Information Fig. S3d). This observation and the known role of IFT proteins in the transport of components in cilia[10], [11], suggested that IFT88 might function in MT transport to poles during mitosis rather than directly participating in MT nucleation at poles.

To test this, we examined the role of IFT88 in the transport of peripheral MT clusters toward spindle poles during the prophase to metaphase transition using GFP-αtubulin-expressing LLC-PK1 cells previously optimized for this purpose[21]. In prometaphase, IFT88 localized to foci at the minus end of peripheral MT clusters where the dynein motor was previously localized[21] (Fig. 3a, Supplementary Information Fig. S4a). In IFT88-depleted cells peripheral MTs clusters accumulated in the cytoplasm (Fig. 3b), suggesting that they were unable to integrate into spindle poles during the prometaphase to metaphase transition. The ectopic MT clusters contained the MT nucleating proteins γtubulin and EB1, and the MT associated motor dynein1 (Fig. 3c, d). To directly test if IFT88 was required for the movement of MT clusters, we examined the recruitment of peripheral MTs to poles by time-lapse imaging (Fig. 3e; Supplementary information movie S1–4 online). In control cells, peripheral MTs moved poleward in prometaphase and contributed to the formation of robust spindle poles, as seen previously (Fig. 3e **top panel**; Supplementary information movie S1)[20], [21]. By metaphase, most clusters were cleared from the periphery and incorporated into spindle poles (Supplementary information movie S2). In IFT88 depleted cells, peripheral MT clusters did not move toward spindle poles in prometaphase (Fig. 3e **lower panel**; Supplementary information movie S3) and by metaphase, they were still not cleared from the periphery (Supplementary Information movie S4), suggesting a defect in transport. An independent strategy that directly tests the movement of MT clusters from periphery to poles during spindle reassembly[26] also revealed a defect in relocalization of MT clusters to poles following IFT88 depletion (Fig. 3f). These results uncover a new role for IFT88 in the movement and subsequent integration of MT clusters containing MT nucleating proteins into spindle poles. They further suggest that IFT88 may be part of a transport complex in mitosis.

MT cluster transport toward spindle poles requires the minus-end directed motor dynein1[21]. In cilia, the movement of IFT88-containing particules is also motor-dependent[11]. We thus asked if IFT88 was part of a MT-based, motor-driven transport system in mitosis as it is in ciliated cells. Consistent with this model, IFT88 co-pelleted with taxol-stabilized MTs from mitotic cell lysates (Fig. 4a). Moreover, the spindle pole localization of IFT88 was dependent on MTs as shown by the dramatic reduction of IFT88 at spindle poles following MT depolymerization, and its restoration after nocodazole washout (Fig. 4b). During spindle reassembly, a remarkable redistribution of IFT88 was observed. Within five minutes, IFT88 redistributed from a diffuse cytoplasmic location to numerous cytoplasmic foci (Fig. 4b). The IFT88 foci contained αtubulin and singular or bundled MTs as well as the newly characterized IFT88 mitotic interacting partners, γtubulin and EB1 (Fig. 4c, d). With time, the number of IFT88 foci decreased concomitant with an increase in the spindle pole fraction (Fig. 4e), suggesting translocation of the cytoplasmic foci to poles. Direct translocation of IFT88 to spindle poles was tested using GFP-IFT88-expressing LLC-PK1 cells (Fig. 4f). GFP-IFT88 localized to spindle poles and to cytoplasmic foci, confirming results with the endogenous protein. GFP-IFT88 foci exhibited vectorial movement toward poles (Supplementary Information, Movie S5; Fig. 4f); anterograde movements were also observed (Fig. 4fII). The speed of IFT88 retrograde movement (>1mm/sec) was consistent with dynein-mediated motility, suggesting that polar transport of IFT88 was mediated by dynein (Fig. 4fII), possibly in the form of a dynein-IFT88 complex. The common functions

of IFT88 and dynein1 in astral MT organization, mitotic spindle orientation (Fig. 1, Fig. 2a, b)[14, 27–29] and transport of MT clusters (Fig. 3)[21] supported this model.

To directly test for the presence of a mitotic IFT88 transport complex, we performed a series of biochemical experiments. The approximate size of mitotic IFT88 complexes was determined by gel filtration (Fig. 5a). IFT88 was detected in fractions 16 to 20 (~2–5 MDa) where it partially co-eluted with dynein1; a separate peak of IFT88 appeared in fraction 26 (~600kDa). Dynein co-eluted with dynactin components (fractions 16 to 22), suggesting that the integrity of the dynein/dynactin complex was retained during gel filtration (Fig. 5a). The partial co-elution of IFT88 and dynein suggested that a subfraction of IFT88 may interact with a subfraction of dynein in a large 2–5 MDa complex (Fig. 5a). In fact, IFT88 and dynein co-immunoprecipitated from mitotic lysates (Supplementary Information Fig. S4b, c). Immunoprecipitation experiments performed on gel filtration fractions containing dynein confirmed that the interaction was maintained after gel filtration (Fig. 5a, **right),** providing further evidence for an IFT88-dynein1 complex in mitosis. Additional IFT proteins co-eluted with IFT88 in the 2–5 MDa range and an interaction between IFT88 and IFT52 (another IFT B-complex component) was identified in mitotic cells (Fig. 5a; Supplementary Information, Fig. S4d, e). These data suggest that IFT88 and maybe other IFT proteins are part of a large dynein1-containing protein complex during mitosis.

To test for a role of dynein1 in the spindle pole localization of IFT88, dynein1 heavy chain was depleted by siRNA. An increase in mitotic index[29] and interphase defects[30] were observed (Supplementary Information, Fig. S5), validating the efficacy of the siRNA. In addition, dynein1 depletion induced a unique redistribution of IFT88 from its focused spindle pole position to a more diffuse region surrounding the poles (Fig. 5b–d), but did not dramatically affect the centrosome localization of IFT88 in interphase as previously reported[6] (Supplementary Information, Fig. S6a). The IFT88 localization pattern was unlike other spindle pole proteins, which were lost from poles but not redistributed (Supplementary Information, Fig. S6b). This observation and the fact that IFT88 misolocalization occurred before major spindle disruption (Supplementary Information, Fig. S6c, d), indicated that IFT88 mislocalization was not due to global perturbations of the spindle. The mitotic redistribution of IFT88 following dynein1 depletion was reminiscent of IFT88 accumulation at cilia tips following depletion of the cilia-associated dynein2 motor[12], an apparent consequence of net MT plus-end motor activity in the absence of minus-end activity (Fig. 5d). A similar redistribution of IFT88 was observed following depletion of p50 dynactin, which disrupts dynein function[29] (Supplementary Information, Fig. S6e–g). In contrast, depletion of the dynein2 motor which is required for retrograde transport in cilia[11, 12], did not affect mitotic index, spindle organization or the spindle pole localization of IFT88 despite its robust interphase and ciliary phenotypes[31] (Supplementary Information Fig. S5, S7). These data demonstrate a role for cytoplasmic dynein1 in the MT-dependent spindle pole localization of IFT88 and suggest that IFT88 functions as part of a previously uncharacterized dynein1-driven complex in mitotic cells.

To directly test the role of dynein1 in IFT88 transport to spindle poles, we examined the translocation of IFT88 foci from cytoplasm to poles during spindle reassembly (Fig. 5e, f). In dynein-depleted cells, IFT88 foci were delayed in their relocalization, as demonstrated by

an increase in the number of IFT88 foci remaining in the cytoplasm after MT regrowth and a decrease in IFT88 at spindle poles (Fig. 5e). More specifically, thirty minutes after nocodazole washout, most (85%) control cells lacked cytoplasmic foci and showed IFT88 at poles, whereas half of the dynein1 depleted cells still showed cytoplasmic IFT88 foci and weak pole staining (Fig. 5f). This demonstrates that dynein1 is required for the transport of IFT88 to spindle poles.

This work identifies a role for an IFT protein in the formation of mitotic astral MT arrays and thus establishes a new molecular mechanism for a cilia protein in spindle orientation. These results, together with the previously-established role of dynein1 in transporting peripheral MTs[21] and centrosome components[32] to spindle poles, suggests that an IFT88-dynein1 complex transports peripheral MT clusters and associated MT nucleating components to spindle poles (model, Fig. 5g). These MT clusters can be viewed as “pre-fabricated” parts of the spindle pole, an observation reminiscent of “pre-assembled” cilia components transported by motors along the cilia[11]. Integration of MT clusters into spindle poles instantly contributes to the astral MT population while the MT nucleating components present in these structures (γtubulin, EB1) could contribute to MT nucleation at poles. Collectively, these events facilitate formation of astral MT arrays and subsequently spindle orientation. The IFT88-mediated spindle pole assembly pathway provides new insight into the underpinnings of fundamental processes including cystogenesis and asymmetric cell division[33].

Because cilia disassemble before mitotic entry[34], the role of IFT88 in the formation of mitotic astral MT arrays represents a novel cilia-independent function for this protein, in addition to its role in cilia formation[3], cell cycle progression[6] and membrane trafficking[35]. The spindle pole localization of several other IFT proteins[5–8] and the mitotic interaction between IFT52 and IFT88 (Supplementary Information, Fig. S4d, e) suggest that other IFT proteins, and maybe other classes of cilia proteins, may function in dividing cells. Moreover, the anterograde movement of IFT88 foci, suggest a role for MT plus-end directed motors in IFT88 mitotic transport (Fig. 4f; Fig. 5d).

IFT88 depletion primarily affects a subset of MTs in mitosis (astrals) consistent with the selective disruption of spindle function. The observed delay in mitosis, rather than a complete mitotic block, indicates that there are no major, potentially fatal defects in spindle function. IFT88 may thus operate selectively in cells, tissues and organisms that require astral MTs for proper spindle orientation, such as the oriented cell divisions in an epithelial layer or the asymmetric division of stem cells[33]. This may explain why IFT88 disruption is not associated with more severe phenotypes in mouse, *Drosophila* or *C. elegans* embryos, such as lethality in the earliest embryonic stages[16, 17, 19].

Cystogenesis has been associated with cilia disruption and misoriented cell division[2]. Despite the appeal for a role of cilia in regulating the planar cell polarity[36], the molecular mechanism leading to misoriented cell division remains unclear. This work provides a likely mechanism for IFT88 function in oriented cell divisions. Additional work is required to test whether the pathway outlined here for IFT88 can be applied to other cilia proteins involved in cystogenesis.

Methods

Cell culture, siRNAs, transfection

HeLa cells, hTert RPE-1 (Clontech, Mountain View, CA) cells, GFP-αtubulin LLC-PK1 stable cell line[20], [21] (Gift from P. Wadsworth), wt or *Tg737* −/− mouse kidney cells[37] and Flag-IFT52 IMCD[38] or GFP-IFT88 LLC-PK stable cell line (Gifts from G. Pazour) were grown as described by American Type Culture Collection (Manassas, VA). Targeted proteins were depleted with small-interfering RNAs (siRNAs) designed and ordered via Dharmacon (Lafayette, CO) and delivered to HeLa or LLC-PK1 cells using Oligofectamine or RPE cells using Lipofectamine 2000 (Invitrogen, Carlsbad, CA) according to manufacturers' instructions. Three siRNA sequences were used to target human and porcine IFT88: IFT88: CGACUAAGUGCCAGACUCAUU, IFT88#2: CCGAAGCACUUAACACUUA previously published [6] and IFT88sc (*Sus Scrofa*): CCUUGGAGAUCGAGAGAAUU. The efficacy of IFT88 knock down was assessed by immunoblotting and immunofluorescence 48h post-transfection. Functional loss of IFT88 was verified using a cilia formation assay in RPE cells[39]. Rescue experiment was performed by depleting endogenous IFT88 (IFT88sc siRNA) in porcine LLC-PK1 cell line expressing a mouse GFP-IFT88 cDNA. EB1 siRNA (GCCCUGGUGUGGUGCGAAA), p50 siRNA (GACGACAGUGAAGGAGUCAUU) and siRNA specific for Dynein1 or Dynein2 (Dharmacon Smart Pool; sequences available upon request) were also used. Control siRNA were described previously (GFP, Lamin)[39]. The efficacy of Dynein 1 and 2 knock down was assessed by RT-PCR (DYNC1H1 FW: GGAAGTCAACGTCACCACCT; DYNC1H1 RV: CCAACCTCAGACCAACCACT; DYNC2 FW: GTCAGCTGGAGGAAGACTGG; DYNC2 RV: GCACCAACAATTTTGTCACG; GAPDH FW: CGACCACTTTGTCAAGCTCA; GAPDH RV: AGGGGAGATTCAGTGTGGTG) using OneStep RT-PCR kit (QIAGEN, Valencia, CA) for both dynein1 and dynein2 and by Western blot for Dynein1. Functional assays for loss of Dynein 1 and 2 were done 48h and 72h post-transfection and included golgi fragmentation (dynein1 and 2) and mitotis-related (dynein1) or cilia assays (dynein2) previously described[39].

Zebrafish lines, MO injection and phenotyping

Wild-type zebrafish were raised according to standard protocols[40]. 1-Phenyl-2-thiourea (PTU, Sigma, St Louis, MO) was used to suppress pigmentation when necessary according to standard protocols[40]. Embryos were staged according to hours post-fertilization (hpf). IFT88 morpholino antisense oligonucleotides (IFT88 MO: CTGGGACAAGATGCACATTCTCCAT) previously described [18] and standard control MO were used. The efficacy of IFT88 MO injection was assessed by changes in gross anatomical features (e.g. curly trunk and pronephric duct defects, cyst formation) characteristic of IFT88 zebrafish mutants[4], [18]. Gross anatomical defects and cyst formation were observed in 32hpf and 52hpf embryos, with a MZFLIII dissection microscope (Zeiss, Thornwood, NY). One cell stage embryos were injected with 10ng of control or IFT88 MO as previously described[18]. 52hpf embryos were used for whole mount staining or flow cytometry (see below).

Antibodies

The following antibodies were used: IFT88 from G. Pazour or Proteintech, Chicago, IL for biochemistry (western blot 1/500, Immunoprecipitation, 5μg) or from C. Desdouets (immunofluorescence 1/250); IFT20 (G. Pazour, western blot 1/500); IFT52 (western blot 1/500, Proteintech, Chicago, IL); polyglutamylated tubulin antibody (GT335, P. Denoulet and C. Janke, immunofluorescence 1/500); αtubulin (DM1α, immunofluorescence 1/250), FITC conjugated αtubulin (1/300), γtubulin (western blot 1/500, immunofluorescence 1/250), EB1(immunofluorescence 1/250, immunoprecipitation 5μg), BrdU (1/250), Flag (western blot 1/500, IP 5μg) and acetylated tubulin (1/250) from Sigma (St Louis, MO); Ser10 Phos-H3 (1/500, Upstate Biotechnology, Lake Placid, NY); EB1 (western blot 1/300, immunofluorescence 1/250), p150 glued (western blot 1/1000), p50/dynactin (western 1/500) from BD Biosciences (Franklin Lakes, NJ), Dynein IC 74.1 (immunofluorescence 1/250, western blot 1/500, IP 5μg, Santa Cruz Biotechnology, Santa Cruz, CA), Golgin 97 (immunofluorescence 1/250, Molecular Probes, Carlsbad, CA), CREST (immunofluorescence 1/250, anti- human centromere/kinetochore; Antibodies Inc. Davis, CA). 5051 (immunofluorescence 1/500) has been described previously[39].

Lysates, cell synchronization, immunoprecipitation and gel filtration

Cell lysates were obtained from HeLa cells 48h or 72h post siRNA transfection. Lysis buffer: 50mM Hepes (pH 7.5), 150mM NaCl, 1.5mM $MgCl_2$, 1 mM EGTA, 1% IGEPAL CA-630, and protease inhibitors (Complete Mini, Roche Diagnostics, Mannheim, Germany). Protein concentration for lysate was determined using Bio-Rad protein dye reagent (Bio-Rad Laboratories, Hercules, CA), loads were adjusted, proteins were resolved by SDS-PAGE, and analyzed by Western Blot. Cell synchronization for biochemistry was achieved using double thymidine block in HeLa cells (2mM, 20h) and release (10h) to achieve mitotic enrichment followed by mitotic shake off. IMCD cells were synchronized in mitosis using R0-3306 inhibitor (Reversibly arrests cells at the G_2-M border, Enzo Life Sciences AG, Switzerland) overnight then released for one hour. For immunoprecipitation, antibodies were added to cell extracts and incubated at 4°C overnight then incubated for 45 min with protein G-PLUS agarose (Santa Cruz Biotechnology, Inc.). Immunoprecipitated proteins were separated by SDS-PAGE and analyzed by western blotting. For gel filtration, mitotic cell lysates (Lysis buffer: 20mM Hepes pH 7.6, 5mM MgSO4, 0.5mM EDTA, and 50mM KCl, 1% NP-40; Volume:0.250 ml; Protein concentration: 12μg/μl) were loaded onto a fast protein liquid chromatography Superose 6 gel-filtration column (GE Healthcare, Piscataway, NJ; 0.2 ml/min, equilibrated in extraction buffer), and 0.5 ml fractions were collected.

Flow cytometry

For flow cytometry, 52hpf zebrafish embryos were grown in egg water and dechorionated by pronase treatment[40], rinsed for 15 minutes in calcium free Ringer and passed several times through a 200μL pipet tip to remove the yolk. Embryos were transferred into a 35 mm culture dish with 2 mL phosphate buffered saline (PBS, pH 8) containing 0.25% trypsin and 1mM EDTA and incubated for 30 to 60 min at 28.5°C. The digest was stopped by adding $CaCl_2$ to a final concentration of 1 mM and fetal calf serum to 10%. Cells were centrifuged for 3 min at 3000 rpm, rinsed once with PBS and fixed and processed for flow cytometry.

Cells were stained for flow cytometry experiments as previously described[39]. Phos-H3 staining (Ser10 Phospho-Histone 3, alexa fluor 488 conjugate), was performed according to manufacturers' instructions (Cell Signaling, Boston, MA).

Microtubule binding assay

Mitotic cells were lysed at 4°C in 100 mM 1,4-piperazinediethanesulfonic acid, pH 6.8, 1 mM $MgCl_2$, 2 mM EGTA, and 1% Triton X-100 and spun 13,000 × *g* for 30 min. Microtubule affinity experiments were performed as described[32] with some modifications. Briefly, purified tubulin (10μg), DTT (1mM), GTP (1 mM) and taxol (10 μM) were added to cleared lysates, and incubated for 1h at 37°C. 10μM nocodazole was added for negative control. Lysates were layered over a 20% sucrose cushion in the above buffer and spun at 100,000*g* for 1h at room temperature. MT pellets were collected after removing lysate and cushion, and bound proteins were separated by SDS-PAGE and analysed by Western blot.

Microtubule regrowth assay

48h post transfection, MTs were depolymerized in 10–25 μM nocodazole in culture medium for 1 hour at 37°C. Cells were then washed and incubated in culture medium without nocodazole at 37°C to allow regrowth. Cells were fixed at different time intervals in MeOH and processed for immunofluorescence to examine MT regrowth (αtubulin) from spindle poles in metaphase cells.

Immunofluorescenc experiments, microscopy and imaging software

48h whole embryos were processed for immunofluorescence by fixation in Dent's Fix (80% methanol/20% DMSO) at 4°C overnight, rehydrated, washed with PBS containing 0.5% Tween 20 (PBST), and blocked in 1X PBS-DBT (1% DMSO, 1% BSA, 0.5% Tween20) at room temperature for 2 hours. Primary and secondary antibody incubations were performed in 1X PBS-DBT at 4°C overnight and 1h at room temperature respectively using 1X PBS-DBT washes between incubations. After rinsing in 1X PBS, the embryos were mounted and examined using a Perkin Elmer Ultraview spinning disk confocal microscope: Zeiss Axiovert 200M, 100x Plan-APOCROMAT NA1.4 Oil, or 63x Plan-APOCROMAT NA1.4 Oil and Hamamatsu ORCA-ER camera. Images were processed on a MetaMorph workstation (Molecular Devices, Downington, PA). Z stacks were acquired and used for creation of maximum projections or 3D rendering (below).

Immunofluorescence analysis of −20°C methanol-fixed cells was performed as previously described[39]. Images were acquired using the spinning disk confocal microscope described above (100x Plan-APOCROMAT NA1.4 Oil). Z stacks were displayed as two-dimensional maximum projections (MetaMorph) or processed for 3-D rendering (Imaris, Bitplane, Saint Paul, MN). Fluorescence range intensity was adjusted identically for each series of panels. Intensity profiles, linescan histograms and fluorescence intensity quantification were obtained from sum projections of Z stacks using MetaMorph. For fluorescence intensity quantification, computer generated concentric circles of 60 (inner area) or 80 (outer area) pixels in diameter were used to measure spindle pole (inner area) and calculate local background (difference between the outer and inner area) fluorescence intensity. Imaris 3D rendering software was used to visualize spindle orientation and to measure distances

required to calculate spindle angle. Spindle angle measurements were performed as previously described [15].

Time-lapse imaging

Time-lapse imaging of cultured HeLa cells was performed using the spinning disk microscope described above (25x Plan-NEOFLUAR NA0.5, phase) using scan stage tool (MetaMorph). Images were taken every 10 min from 32h to 48h post transfection. For live microscopy of GFP-EB1 in metaphase HeLa cells, images were recorded every 5 seconds for 2 minutes using the spinning disk confocal microscope described above (63x Plan-APOCROMAT NA1.4 Oil). MT nucleation rate was measured in GFP-EB1 cells by manually counting the number of EB1-GFP comets emerging from the centrosome over time. For live microscopy of GFP-IFT88 in metaphase, single plane images were recorded once per second using the spinning disk confocal microscope described above (100× Plan-APOCROMAT NA1.4 Oil). Resulting movie is displayed at 3 frames per second. Tracking of IFT88 foci was obtained using the track point application in MetaMorph. Live imaging of the GFP-αtubulin LLC-PK1 cell line was performed as previously described[21]. Resulting movies are displayed at 10 frames per second.

Statistical analysis

The number of embryos or cells counted per experiment for statistical analysis is indicated in figure legends. For graphs in all figures: error bars, mean of at least 3 experiments +/− SD unless otherwise specified; n, number of events/experiment. Images: scale bars, 5μm unless otherwise specified. Graphs were created using GraphPad Prism software (San Diego, CA).

Supplementary Material

Refer to Web version on PubMed Central for supplementary material.

Acknowledgments

We thank G. Pazour, G. Witman and P. Wadsworth for thoughtful discussions on this work, S. Redick for assistance with microscopy. We are particularly thankful to Laurence Covassin-Barberis in N.L. laboratory and Nicholas L. Adkins in Craig Peterson's laboratory for guidance on zebrafish experimental work and gel filtration experiments respectively. We thank G. Pazour for the gift of IFT88 antibody and GFP-IFT88 LLC-PK1, Flag-IFT52 IMCD stable cell lines, P. Wadsworth for the GFP-αtubulin LLC-PK1 cell line and C. Desdouets, P. Denoulet and C. Janke for their generous gift of antibodies to IFT88 and polyglutamylated tubulin, respectively. Core resources supported by the Diabetes Endocrinology Research Center grant DK32520 were used; S.D. is a member of the UMass DERC (DK32520). This work was supported by funding from the National Institutes of Health (GM51994) to S.D. and the Polycystic Kidney Disease Foundation to B.D.

References

1. Hildebrandt F, Otto E. Cilia and centrosomes: a unifying pathogenic concept for cystic kidney disease? Nat Rev Genet. 2005; 6:928–940. [PubMed: 16341073]
2. Fischer E, et al. Defective planar cell polarity in polycystic kidney disease. Nat Genet. 2006; 38:21–23. [PubMed: 16341222]
3. Pazour GJ, et al. Chlamydomonas IFT88 and its mouse homologue, polycystic kidney disease gene tg737, are required for assembly of cilia and flagella. J Cell Biol. 2000; 151:709–718. [PubMed: 11062270]

4. Sun Z, et al. A genetic screen in zebrafish identifies cilia genes as a principal cause of cystic kidney. Development. 2004; 131:4085–4093. [PubMed: 15269167]
5. Iomini C, Tejada K, Mo W, Vaananen H, Piperno G. Primary cilia of human endothelial cells disassemble under laminar shear stress. J Cell Biol. 2004; 164:811–817. [PubMed: 15024030]
6. Robert A, et al. The intraflagellar transport component IFT88/polaris is a centrosomal protein regulating G1-S transition in non-ciliated cells. J Cell Sci. 2007; 120:628–637. [PubMed: 17264151]
7. Follit JA, Tuft RA, Fogarty KE, Pazour GJ. The intraflagellar transport protein IFT20 is associated with the Golgi complex and is required for cilia assembly. Mol Biol Cell. 2006; 17:3781–3792. [PubMed: 16775004]
8. Deane JA, Cole DG, Seeley ES, Diener DR, Rosenbaum JL. Localization of intraflagellar transport protein IFT52 identifies basal body transitional fibers as the docking site for IFT particles. Curr Biol. 2001; 11:1586–1590. [PubMed: 11676918]
9. Rieder CL, Faruki S, Khodjakov A. The centrosome in vertebrates: more than a microtubule-organizing center. Trends Cell Biol. 2001; 11:413–419. [PubMed: 11567874]
10. Scholey JM. Intraflagellar transport motors in cilia: moving along the cell's antenna. J Cell Biol. 2008; 180:23–29. [PubMed: 18180368]
11. Rosenbaum JL, Witman GB. Intraflagellar transport. Nat Rev Mol Cell Biol. 2002; 3:813–825. [PubMed: 12415299]
12. Pazour GJ, Dickert BL, Witman GB. The DHC1b (DHC2) isoform of cytoplasmic dynein is required for flagellar assembly. J Cell Biol. 1999; 144:473–481. [PubMed: 9971742]
13. Luders J, Stearns T. Microtubule-organizing centres: a re-evaluation. Nat Rev Mol Cell Biol. 2007; 8:161–167. [PubMed: 17245416]
14. O'Connell CB, Wang YL. Mammalian spindle orientation and position respond to changes in cell shape in a dynein-dependent fashion. Mol Biol Cell. 2000; 11:1765–1774. [PubMed: 10793150]
15. Toyoshima F, Nishida E. Integrin-mediated adhesion orients the spindle parallel to the substratum in an EB1- and myosin X-dependent manner. Embo J. 2007; 26:1487–1498. [PubMed: 17318179]
16. Murcia NS, et al. The Oak Ridge Polycystic Kidney (orpk) disease gene is required for left-right axis determination. Development. 2000; 127:2347–2355. [PubMed: 10804177]
17. Haycraft CJ, Swoboda P, Taulman PD, Thomas JH, Yoder BK. The C. elegans homolog of the murine cystic kidney disease gene Tg737 functions in a ciliogenic pathway and is disrupted in osm-5 mutant worms. Development. 2001; 128:1493–1505. [PubMed: 11290289]
18. Kramer-Zucker AG, et al. Cilia-driven fluid flow in the zebrafish pronephros, brain and Kupffer's vesicle is required for normal organogenesis. Development. 2005; 132:1907–1921. [PubMed: 15790966]
19. Han YG, Kwok BH, Kernan MJ. Intraflagellar transport is required in Drosophila to differentiate sensory cilia but not sperm. Curr Biol. 2003; 13:1679–1686. [PubMed: 14521833]
20. Tulu US, Rusan NM, Wadsworth P. Peripheral, non-centrosome-associated microtubules contribute to spindle formation in centrosome-containing cells. Curr Biol. 2003; 13:1894–1899. [PubMed: 14588246]
21. Rusan NM, Tulu US, Fagerstrom C, Wadsworth P. Reorganization of the microtubule array in prophase/prometaphase requires cytoplasmic dynein-dependent microtubule transport. J Cell Biol. 2002; 158:997–1003. [PubMed: 12235119]
22. Hannak E, et al. The kinetically dominant assembly pathway for centrosomal asters in Caenorhabditis elegans is gamma-tubulin dependent. J Cell Biol. 2002; 157:591–602. [PubMed: 12011109]
23. Rogers SL, Rogers GC, Sharp DJ, Vale RD. Drosophila EB1 is important for proper assembly, dynamics, and positioning of the mitotic spindle. J Cell Biol. 2002; 158:873–884. [PubMed: 12213835]
24. Zimmerman WC, Sillibourne J, Rosa J, Doxsey SJ. Mitosis-specific anchoring of gamma tubulin complexes by pericentrin controls spindle organization and mitotic entry. Mol Biol Cell. 2004; 15:3642–3657. [PubMed: 15146056]
25. Green RA, Wollman R, Kaplan KB. APC and EB1 function together in mitosis to regulate spindle dynamics and chromosome alignment. Mol Biol Cell. 2005; 16:4609–4622. [PubMed: 16030254]

26. Tulu US, Fagerstrom C, Ferenz NP, Wadsworth P. Molecular requirements for kinetochore-associated microtubule formation in mammalian cells. Curr Biol. 2006; 16:536–541. [PubMed: 16527751]
27. Walczak CE, Vernos I, Mitchison TJ, Karsenti E, Heald R. A model for the proposed roles of different microtubule-based motor proteins in establishing spindle bipolarity. Curr Biol. 1998; 8:903–913. [PubMed: 9707401]
28. Gaglio T, Dionne MA, Compton DA. Mitotic spindle poles are organized by structural and motor proteins in addition to centrosomes. J Cell Biol. 1997; 138:1055–1066. [PubMed: 9281583]
29. Echeverri CJ, Paschal BM, Vaughan KT, Vallee RB. Molecular characterization of the 50-kD subunit of dynactin reveals function for the complex in chromosome alignment and spindle organization during mitosis. J Cell Biol. 1996; 132:617–633. [PubMed: 8647893]
30. Corthesy-Theulaz I, Pauloin A, Pfeffer SR. Cytoplasmic dynein participates in the centrosomal localization of the Golgi complex. J Cell Biol. 1992; 118:1333–1345. [PubMed: 1387874]
31. Vaisberg EA, Grissom PM, McIntosh JR. Mammalian cells express three distinct dynein heavy chains that are localized to different cytoplasmic organelles. J Cell Biol. 1996; 133:831–842. [PubMed: 8666668]
32. Young A, Dictenberg JB, Purohit A, Tuft R, Doxsey SJ. Cytoplasmic dynein-mediated assembly of pericentrin and gamma tubulin onto centrosomes. Mol Biol Cell. 2000; 11:2047–2056. [PubMed: 10848628]
33. Yamashita YM, Mahowald AP, Perlin JR, Fuller MT. Asymmetric inheritance of mother versus daughter centrosome in stem cell division. Science. 2007; 315:518–521. [PubMed: 17255513]
34. Rieder CL, Jensen CG, Jensen LC. The resorption of primary cilia during mitosis in a vertebrate (PtK1) cell line. J Ultrastruct Res. 1979; 68:173–185. [PubMed: 480410]
35. Finetti F, et al. Intraflagellar transport is required for polarized recycling of the TCR/CD3 complex to the immune synapse. Nat Cell Biol. 2009; 11:1332–1339. [PubMed: 19855387]
36. Ross AJ, et al. Disruption of Bardet-Biedl syndrome ciliary proteins perturbs planar cell polarity in vertebrates. Nat Genet. 2005; 37:1135–1140. [PubMed: 16170314]
37. Pazour GJ, San Agustin JT, Follit JA, Rosenbaum JL, Witman GB. Polycystin-2 localizes to kidney cilia and the ciliary level is elevated in orpk mice with polycystic kidney disease. Curr Biol. 2002; 12:R378–380. [PubMed: 12062067]
38. Follit JA, Xu F, Keady BT, Pazour GJ. Characterization of mouse IFT complex B. Cell Motil Cytoskeleton. 2009; 66:457–468. [PubMed: 19253336]
39. Mikule K, et al. Loss of centrosome integrity induces p38-p53-p21-dependent G1-S arrest. Nat Cell Biol. 2007; 9:160–170. [PubMed: 17330329]
40. Westerfield, M. The Zebrafish book : a guide for the laboratory use of zebrafish (Brachydanio rerio). University of Oregon Press; Eugene. Or: 1993.

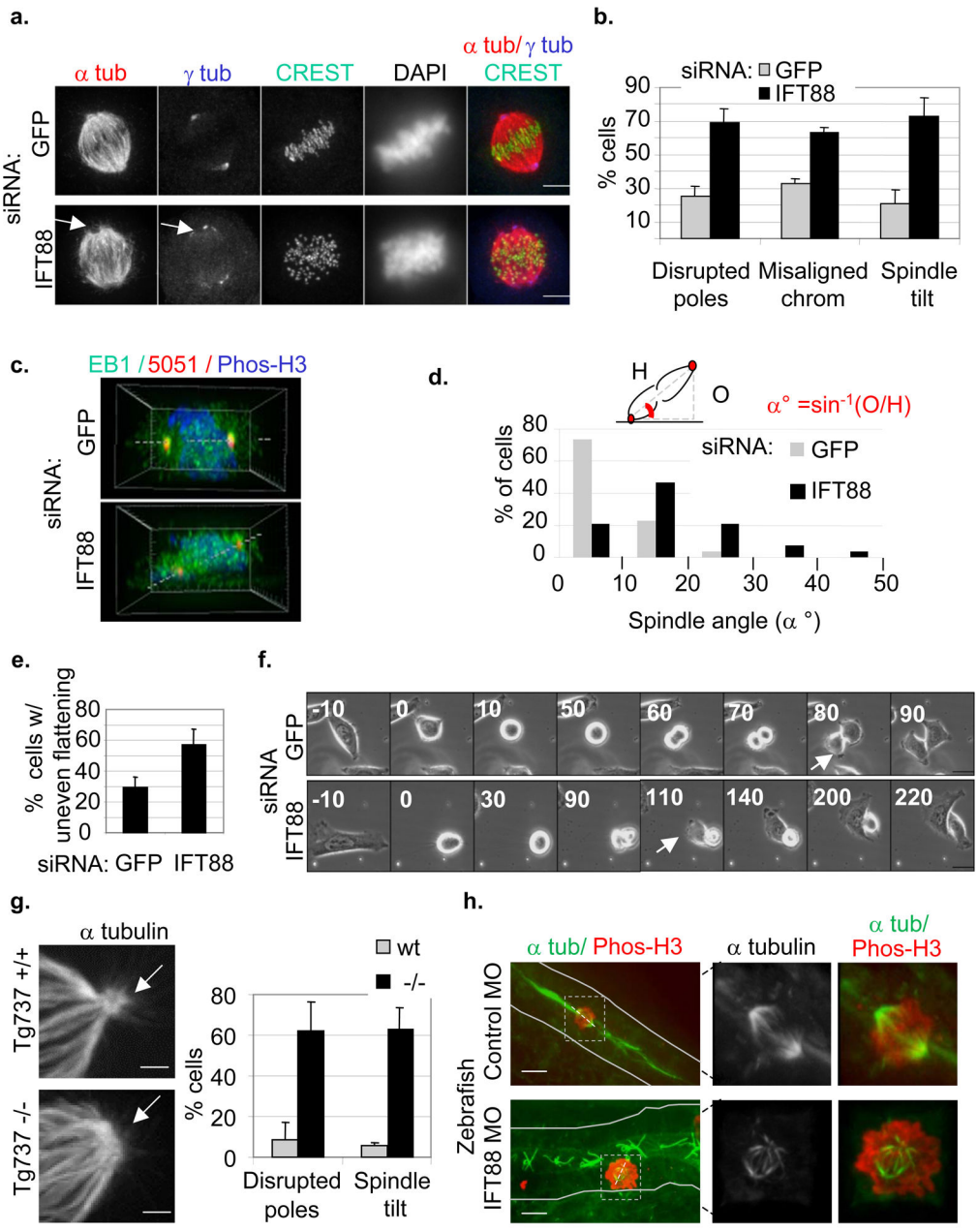

Figure 1. IFT88 depletion leads to mitotic defects in HeLa cells, kidney cells from the *Tg737*^{orpk} mouse mutant and zebrafish

(a) Immunofluorescence images of control (GFP) and IFT88 siRNA-treated mitotic HeLa cells. αtubulin (α tub, MTs) and γtubulin (γ tub, spindle poles, arrow) staining show spindle pole defects. CREST (kinetochores) or DAPI (DNA) staining show misaligned chromosomes. Scale bars, 5μm. **(b)** Quantification of mitotic defects following IFT88 or control (GFP) siRNA treatment in HeLa cells. Defects include disrupted poles (α and γtubulin), misaligned chromosomes (DAPI staining) and spindle misorientation (spindle tilt, spindle poles in different focal planes). n=70 mitotic cells/experiment. **(c–d)** Side views of three-dimensional reconstructed immunofluoresence images (c) show misoriented mitotic

spindles in IFT88 versus control siRNA-treated HeLa cells. Spindle (EB1), centrosomes (5051) and DNA (Phos-H3). Histogram (d) shows metaphase spindle angle distribution in control and IFT88 siRNA-treated cells. n=30 mitotic spindles. Schematic (d, top) shows spindle angle (α) measurement. H, hypotenuse. O, opposite. **(e–f)** Quantification (e) and time-lapse images (f) show uneven timing of daughter cell flattening onto the substrate after mitosis (misoriented cell division) in IFT88 siRNA treated HeLa cells compared to control. n=50 mitotic cells/experiment. Arrows, time when the first daughter cell begins flattening. Time, min. Scale bar, 10um. **(g)** Immunofluorescence images showing a disrupted spindle pole (αtubulin, arrow) in kidney cells derived from the IFT88 mouse mutant *Tg737*^{orpk} (*Tg737*−/−) compared to wt (*Tg737*+/+). Scale bars, 2μm. Graph (right): quantification of mitotic defects in wt and *Tg737*^{orpk} mutant cells. **(h)** Immunofluorescence images of mitotic spindles from the pronephric ducts of whole mount zebrafish embryos. Control embryo, cell with aligned chromosomes and mitotic spindle oriented in the longitudinal plane of the duct. IFT88 depleted embryo, cell with nonaligned chromosomes and misoriented spindle. Lines, pronephric duct border. Dotted lines, spindle orientation. MO, morpholino. Right, enlargements of boxed spindles. Scale bar, 5 μm.

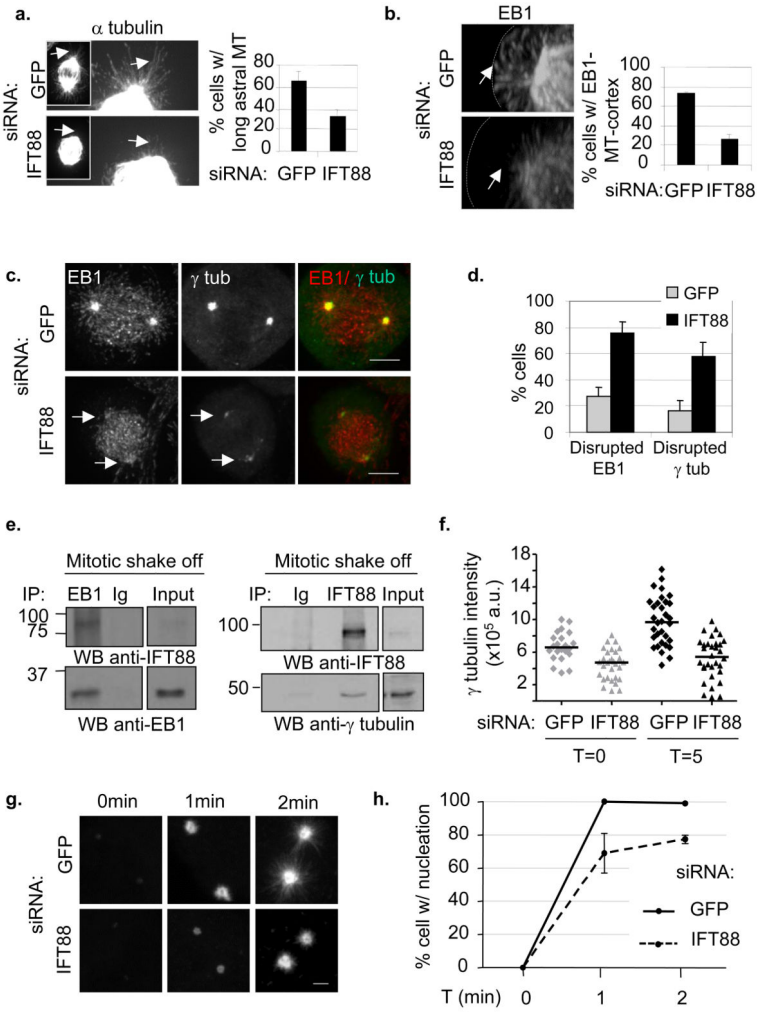

Figure 2. IFT88 depletion disrupts astral MTs and the spindle pole localization of proteins involved in MT nucleation in HeLa cells

(a) Immunofluoresence images of mitotic spindles showing disrupted astral MTs (αtubulin) at spindle poles of IFT88 depleted cells compared to control. Pixel intensity range increased to visualize astral MTs (arrow). Enlargements, spindle pole region. Graph (right), quantification of cells with long astral MTs (>3μm). n=70 mitotic spindles/experiment. **(b)** Side view of three-dimensional reconstructed images showing astral MTs (EB1 staining) contacting the cortex in control cells (arrow, upper panel) and astral MTs which fail to contact the cell cortex in IFT88 depleted cells (arrow, lower panel). Dotted lines, cell cortex. Graph (right): quantification of cells with both poles showing astral MTs contacting cortex. n=50 mitotic spindles/experiment. **(c, d)** Immunofluorescence images (c) and quantification (d) of mitotic spindles showing loss of EB1 and γtubulin (γ tub) from spindle poles (arrow) in IFT88 depleted cells compared to control. Graph (d): % cells with disrupted pole localization of EB1 or γtubulin (γ tub). n=50 mitotic spindles/experiment. Scale bar, 5μm. **(e)** Immunoblots showing that IFT88 co-immunoprecipitates with EB1 (left) and that γtubulin co-immunoprecipitates with IFT88 (right) from lysates of mitotic HeLa cells demonstrating a mitotic interaction between the proteins, either direct or indirect. Ig, rabbit

antibody, negative IP control. Input, 5% of total lysate used for IP. For full scan of immunoblots see Supplementary Fig. S8. **(f)** Quantification of γtubulin intensity at spindle poles of mitotic cells showing γtubulin recruitment to poles in a MT regrowth experiment. T, time after nocodazole washout (min). Bar, median. Experiment shown is representative of three independent experiments. a.u., arbitrary unit. **(g)** Immunofluoresence images showing MT regrowth (αtubulin) at mitotic spindle poles 0min, 1min and 2min after nocodazole washout in IFT88 or GFP depleted mitotic cells. T=0min shows no nucleation in GFP and IFT88 depleted cells, T=1min and 2min show decreased nucleation in IFT88 depleted cells compared to control cells. Scale bar, 2μm. **(h)** % cells showing detectable nucleation (aster size ≥ 1μm) 0min, 1min and 2min after nocodazole washout. n=50 mitotic cells/experiment; error bars, mean of at least 3 experiments +/− SD.

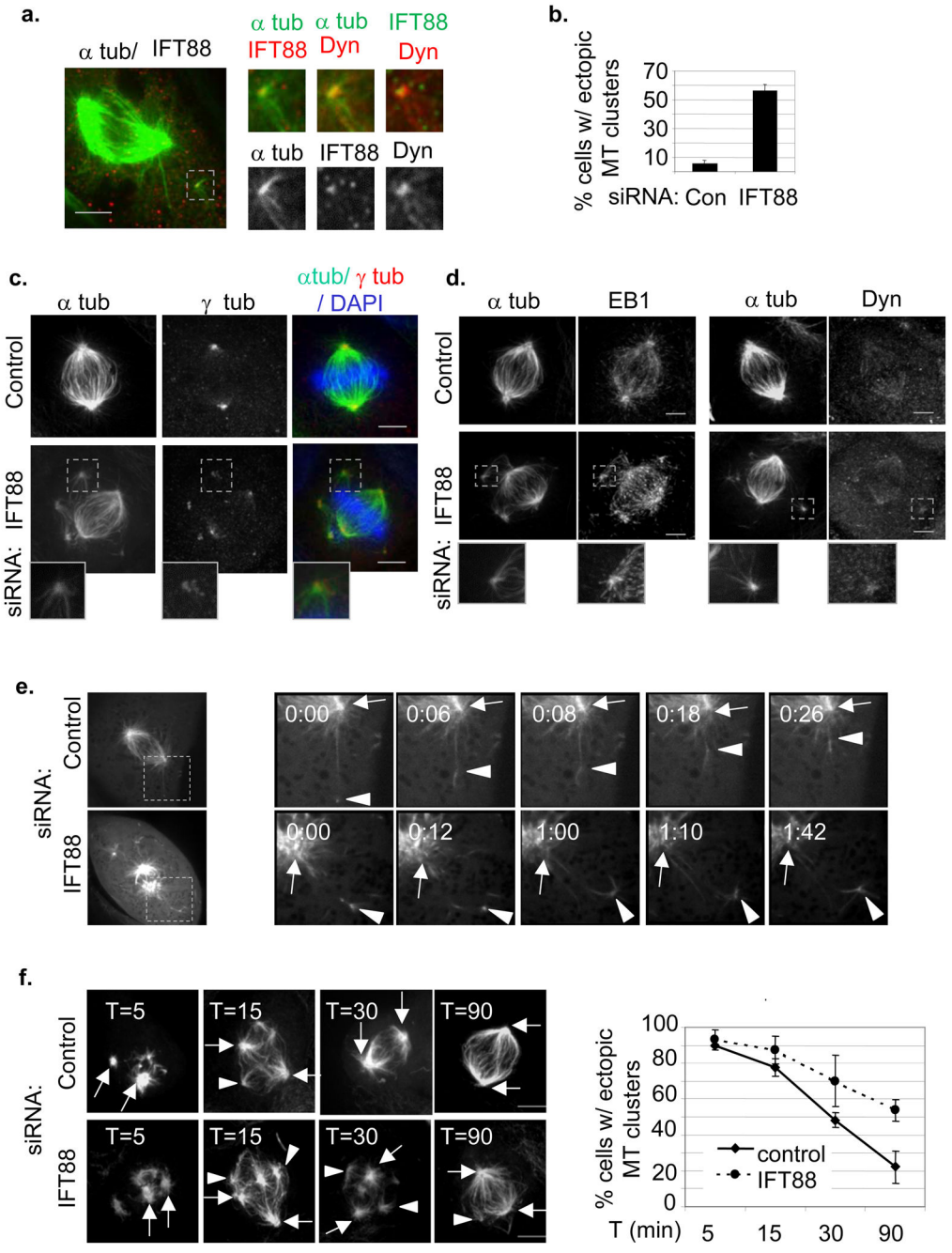

Figure 3. IFT88 is required for the movement of peripheral MT clusters containing MT nucleating components toward spindle poles in LLC-PK1 cells stably expressing GFP-α tubulin

(a) Immunofluoresence images showing IFT88 and dynein (intermediate chain, dynein IC) localizing to a peripheral MT cluster (GFP-αtubulin) in a prometaphase cell. Pixel intensity range increased to visualize peripheral MT cluster. Scale bar, 5μm. Inset, peripheral MT cluster. See Supplementary information Fig. S4a for negative controls. **(b)** Quantification of GFP-αtubulin LLC-PK1 metaphase cells with ectopic MT clusters following IFT88 or control (Con, lamin) siRNA treatment. n=50 mitotic cells/experiment. **(c–d)** Immunofluoresence images of GFP-αtubulin LLC-PK1 control or IFT88 depleted

metaphase cells. γtubulin (c), EB1 (d, left) and dynein (d, right) localize to ectopic MT clusters. Insets, ectopic MT clusters. Scale bar, 5μm. **(e)** Selected still images from time-lapse movies of GFP-αtubulin LLC-PK1 cells. Control prometaphase, minus-end directed motion of peripheral MT clusters toward spindle pole. In IFT88 depleted cells, peripheral clusters formed but showed no movement towards spindle poles. Full cell (left); enlargement of spindle pole and MT cluster (right). Time (min); arrowhead, MT cluster; arrow, spindle pole. **(f)** Immunofluorescence images (left) and quantification (right) of the relocalization of MT clusters to spindle poles in a spindle reassembly assay (αtubulin, MT regrowth following nocodazole washout). The decrease in cells with ectopic MT clusters over time correlates with their movement towards the poles. IFT88 depletion delays relocalization of MT clusters to poles. Arrows, spindle poles (localization confirmed with centrosome protein staining). Arrowheads, ectopic MT clusters. n=40 mitotic cells/experiment/time point. T, time after nocodazole washout (min).

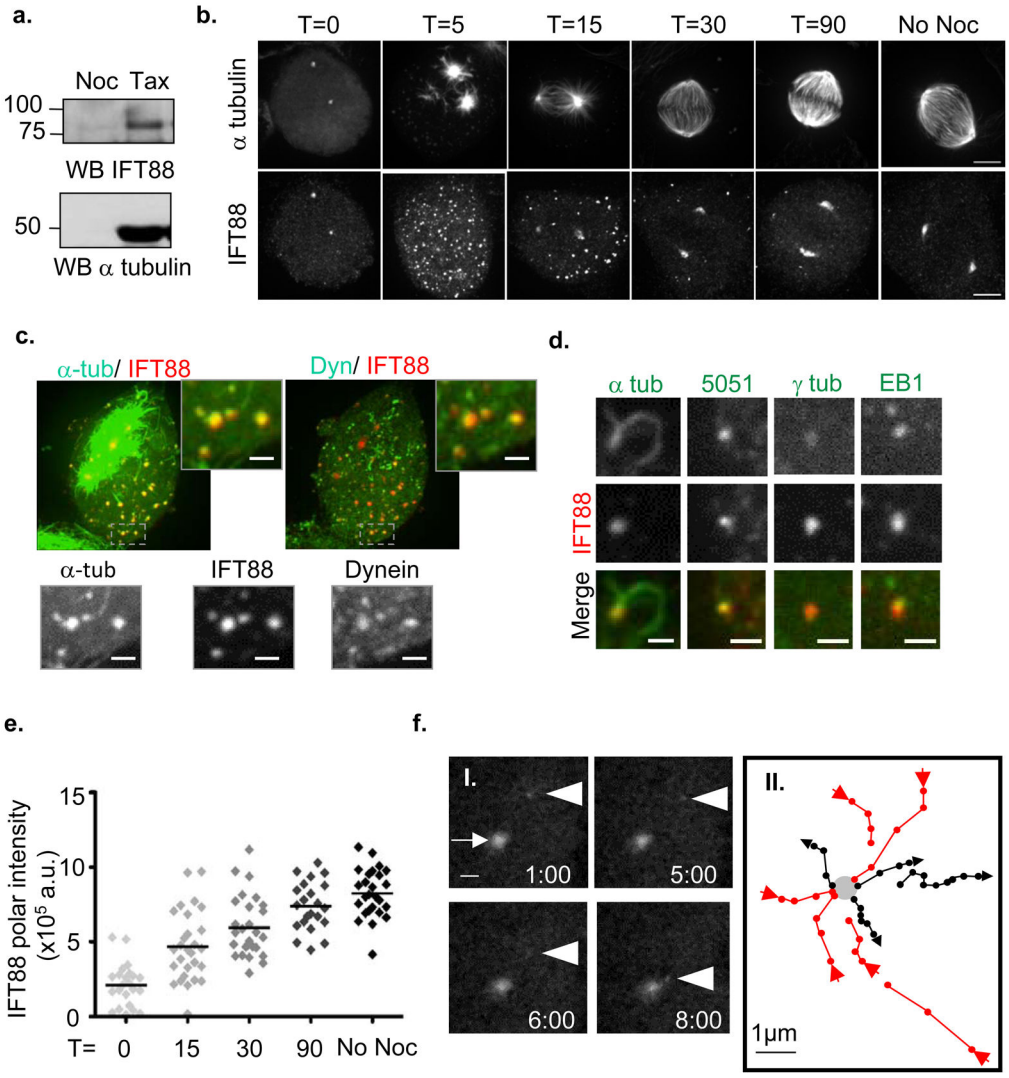

Figure 4. IFT88 moves towards spindle poles and requires MTs for its spindle pole localization

(a) MT pull down assay shows IFT88 co-pelleted with taxol-stabilized MTs (Tax) in mitotic HeLa cell lysates. Nocodazole (Noc), inhibition of microtubule polymerization used as negative control. αtubulin, MTs **(b)** Immunofluoresence images showing IFT88 foci formation (lower panel) after nocodazole washout (αtubulin, MT regrowth; upper panel) in HeLa cells. T, time after nocodazole washout (min). Control without nocodazole (no noc). Scale bar, 5μm. **(c, d)** Immunofluorescence images showing the molecular composition of IFT88 foci in HeLa cells. Maximum projection of a cell with IFT88 foci 5min after nocodazole washout (c) shows that IFT88 foci co-stain for αtubulin and dynein intermediate chain (Dyn). Enlargments, single plane of the boxed foci. Enlargements of IFT88 foci (d) showing that MT clusters can be observed extending from the foci, and that IFT88 foci costain with MT nucleating components (5051, centrosome protein marker; γtubulin; EB1). Pixel intensity range increased to visualize foci. Scale bar, 1μm. **(e)** Quantification of IFT88 intensity at spindle poles of mitotic HeLa cells showing IFT88 recruitment to poles following nocodazole washout. T, time after nocodoazole washout (min). Experiment shown

is representative of three independent experiments. Bar, median. a.u., arbitrary unit. No nocodazole (No Noc), untreated cells. **(f)** Still images from time-lapse imaging of a GFP-IFT88 LLC-PK1 cell line (I.) showing one of the GFP-IFT88 foci (arrowhead) moving toward the GFP-IFT88-labeled spindle pole (arrow). Time elapsed is shown in seconds. Scale bar, 1μm. Schematic representation (II.) of several GFP-IFT88 foci moving toward (red arrow) or away from (black arrowhead) the spindle pole (grey dot). Time between points, 1second. Arrows indicate the direction of the movement.

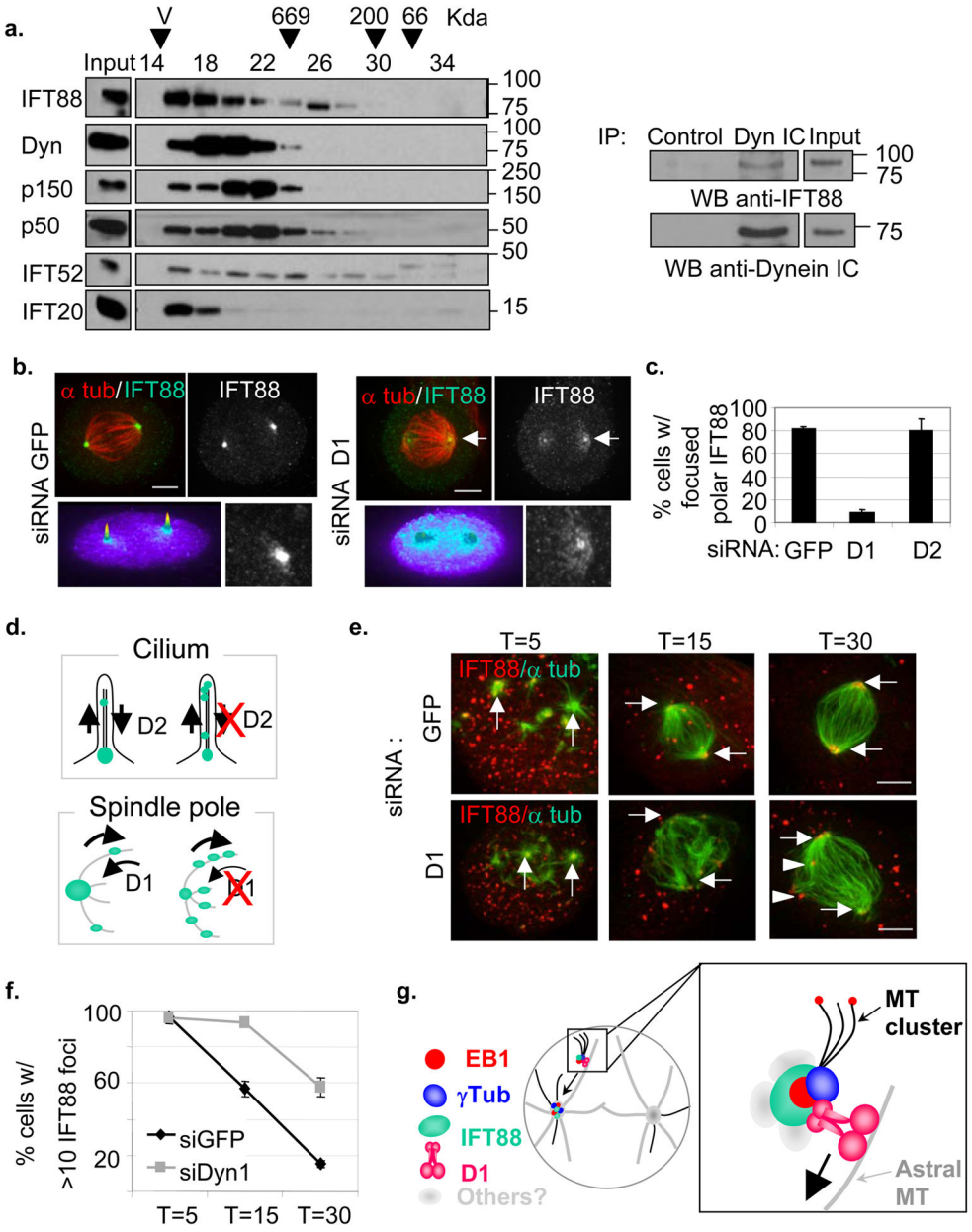

Figure 5. IFT88 is part of a dynein1-driven transport complex in mitosis

(a) Immunoblots (left) showing fractions of mitotic HeLa cell lysates obtained after gel filtration fractionation and probed for IFT88, dynein intermediate chain, dynactin p150/glued, p50 dynactin, IFT52 and IFT20. Input, total lysate before gel filtration. Arrowheads, peak elution fraction for calibration proteins: BSA (66kDa), β-amylase (200kDa), thyroglobulin (669kDa). V, Void volume. Immunoprecipitation experiment (right) performed on fractions 16 to 22 from gel filtration containing dynein. Immunoblots show that IFT88 co-immunoprecipitates with dynein (IC, intermediate chain) after gel filtration. For full scan of immunoblots see Supplementary Fig. S8. **(b–d)** Immunofluorescence images of HeLa cells (b) showing IFT88 redistribution from mitotic spindle poles to a more diffuse

region surrounding the poles following dynein1 (D1) depletion compared to control (GFP). αtubulin (α tub). Intensity profiles, lower left panels; Spindle pole enlargement, lower right panels. Scale bar, 5μm. Graph (c), % cells with focused IFT88 localization at poles following dynein1 (D1) or dynein2 (D2) siRNA treatment. n=70 mitotic spindles/ experiment. Schematic representation (d) of IFT88 (green) redistribution in cilia when D2 is depleted, and around mitotic spindle poles when D1 is depleted. **(e, f)** Immunofluorescence images (e) showing that D1 depletion in HeLa cells delays IFT88 (red) relocalization to spindle poles in a spindle reassembly assay (αtubulin, green). The decrease of cytoplasmic foci over time, observed in control (GFP) cells correlates with the relocalization of IFT88 from foci to spindle poles. Despite the formation of MT clusters in D1 depleted cells, several IFT88 foci remain in the cytoplasm 30 min after nocodazole washout. Arrows, spindle poles; Arrowheads, IFT88 foci. Graph (f): % of cells with more than ten cytoplasmic foci. n=40 cells/experiment/time point. T, time after nocodazole washout (min). **(g)** Molecular model for IFT88 function in mitosis. IFT88 is depicted as a component of a minus-end directed dynein1-driven transport complex. This complex is required for transport of MT clusters and their associated nucleating components (EB1 and γtubulin) to spindle poles. IFT88 thus contributes to the formation of astral MT arrays and consequently spindle orientation. Adapted from[20].